Engineering 7 (2021) 630–635

Contents lists available at ScienceDirect

Engineering

journal homepage: www.elsevier.com/locate/eng

Research
Green Chemical Engineering: Soft Matter—Letter

Nanobubble Dynamics in Aqueous Surfactant Solutions Studied by Liquid-Phase Transmission Electron Microscopy

Yuna Bae [a,b], Sungsu Kang [a,b], Byung Hyo Kim [a,b,d], Kitaek Lim [c], Sungho Jeon [c], Sangdeok Shim [e,*], Won Chul Lee [c,*], Jungwon Park [a,b,*]

[a] School of Chemical and Biological Engineering, and Institute of Chemical Processes, Seoul National University, Seoul 08826, Republic of Korea
[b] Center for Nanoparticle Research, Institute of Basic Science (IBS), Seoul 08826, Republic of Korea
[c] Department of Mechanical Engineering, BK21 FOUR ERICA-ACE Center, Hanyang University, Ansan 15588, Republic of Korea
[d] Department of Organic Materials and Fiber Engineering, Soongsil University, Seoul 06978, Republic of Korea
[e] Department of Chemistry, Sunchon National University, Suncheon 57922, Republic of Korea

ARTICLE INFO

Article history:
Received 11 September 2020
Revised 17 December 2020
Accepted 8 February 2021
Available online 31 March 2021

Keywords:
Nanobubbles
In situ TEM
Liquid-phase TEM
Surfactant

ABSTRACT

Nanobubbles have attracted considerable attention in various industrial applications due to their exceptionally long lifetime and their potential as carriers at the nanoscale. The stability and physiochemical properties of nanobubbles are highly sensitive to the presence of surfactants that can lower their surface tension or improve their electrostatic stabilization. Herein, we report real-time observations of the dynamic behaviors of nanobubbles in the presence of soluble surfactants. Using liquid-phase transmission electron microscopy (TEM) with multi-chamber graphene liquid cells, bulk nanobubbles and surface nanobubbles were observed in the same imaging condition. Our direct observations of nanobubbles indicate that stable gas transport frequently occurs without interfaces merging, while a narrow distance is maintained between the interfaces of interacting surfactant-laden nanobubbles. Our results also elucidate that the interface curvature of nanobubbles is an important factor that determines their interfacial stability.

1. Introduction

Nanobubbles have a wide range of industrial applications, such as surface cleaning [1], water treatment [2–4], and biomedical research [5,6], due to their remarkable long-term stability on solid substrates and in liquid media [7–9]. In classical thermodynamics, it is believed that the bubbles quickly shrink within microseconds as their size approximates the nanoscale, because the interior Laplace pressure is too high to prevent the outward diffusion of the gas inside the bubble [10,11]. Nonetheless, diverse experimental approaches, such as atomic force microscopy (AFM) and cryo-electron microscopy (cryo-EM), have been utilized to confirm the existence and origins of the long-term stability of nanobubbles [12–15]. The results of these studies suggest that nanobubble stability is significantly enhanced on surfaces due to the pinning effect of the three-phase contact line [16–18].

It is expected that the size and stability of nanobubbles can be actively controlled by manipulating their interfacial chemistry. Similar to the case of fluid interfaces constructed at the micrometer scale and beyond [19–21], the choice of surfactant additive influences the different chemical structures of the interfacial boundaries and surface charge states, which alter the lifetime of nanobubbles and inter-nanobubble interactions [22]. Computational simulations have demonstrated that the addition of amphiphilic or insoluble surfactants lowers the stability of nanobubbles by disturbing the pinning process and reducing surface tension [23]. In contrast, anionic surfactants generate surface charges on nanobubbles that promote electrostatic stabilization, while suppressing nanobubble merging [24].

Liquid-phase transmission electron microscopy (TEM) achieves nanoscale spatial resolution for *in situ* visualizations of the chemical and physical processes occurring in a liquid environment [25–28]. Thus, it has been recently applied for real-time and real-space observations of changes in gas–liquid interfaces and of the behavior of nanobubbles in pure water and protein solutions [29–33]. The formation of nanobubbles produced by electron-beam-

* Corresponding authors.
E-mail addresses: san90@scnu.ac.kr (S. Shim), wonchullee@hanyang.ac.kr (W.C. Lee), jungwonpark@snu.ac.kr (J. Park).

https://doi.org/10.1016/j.eng.2021.02.006

induced radiolysis and inter-bubble gas transport has been investigated [34]. Furthermore, microscopic results have indicated the existence of a critical radius of stable nanobubbles in pure water [35]. Here, we study the dynamic phenomena of surfactant-laden nanobubbles in an aqueous solution by employing multi-chamber graphene liquid cell TEM, wherein the chemical conditions for encapsulated solution samples are reliably maintained during multiple *in situ* observations.

2. Materials and methods

2.1. Fabrication of a multi-chamber graphene liquid cell

A highly ordered array of graphene-covered nano-chambers was prepared by assembling a porous anodic aluminum oxide (AAO) membrane between two graphene sheets, as developed in our previous study [36]. First, a set of graphene-transferred TEM grids was prepared for use as the top and bottom graphene windows [37]. The AAO membrane (on a poly(methyl methacrylate) (PMMA) substrate), with a pore diameter of 80 nm, an inter-pore distance of 125 nm, and a thickness of 50 nm, was cut to fit the inner square size of the TEM grid. A drop of water was dispensed on a prepared graphene-transferred grid, and a square AAO membrane was placed on this grid in a direction wherein the exposed AAO surface faced the droplet. After drying the assembled grid in an oven for 5 min at 70 °C, the AAO membrane attached to the graphene sheet via van der Waals interactions. The assembled grid was immersed in an acetone bath for 4 h to remove the PMMA substrate that supported the AAO membrane, thereby producing a nano-well-shaped array built on the bottom grid. A 0.5 μL liquid sample was loaded onto the fabricated nano-well-shaped array, which was then covered with another graphene-transferred grid to construct the multi-chamber liquid cell. Each cylindrical nanochamber built on the liquid cell consisted of a nanopore and top/bottom graphene sheets encapsulating the liquid sample. In this study, a 3.75 mmol·L^{-1} aqueous solution of hexadecyltrimethylammonium bromide (CTAB) was used as a liquid sample. A 2.5 mmol·L^{-1} chloroauric acid solution was also added to the liquid sample because the reduction of this acid solution to form gold nanoparticles can be used as an indicator for successful liquid encapsulation during electron-beam irradiation. It should be noted that the *in situ* observations of surfactant-laden nanobubbles were conducted in regions away from the gold nanoparticles. The multi-chamber graphene liquid cell can improve the stability of the liquid system and ensure encapsulation of the liquid sample with a defined dimension and volume, resulting in reliable fluid mechanics during the observations. In addition, the stable and sufficient space of the nanochamber makes it possible to observe the dynamic phenomena of bulk nanobubbles under weak perturbation by graphene or a confined environment.

2.2. TEM analysis

We observed the nanobubbles in aqueous surfactant solutions by means of liquid-phase TEM with the fabricated multi-chamber graphene liquid cell (Appendix A Movies S1–5). Nanobubbles were imaged using a JEM-2100F (JEOL Ltd., Japan) instrument operating at 200 kV and equipped with an UltraScan 1000XP CCP detector (Gatan, Inc., USA). *In situ* TEM movies were recorded at 7.5 frames per second (fps). The dose rate of the electron beam was consistently maintained at 1800–2000 e·Å^{-2}·s^{-1}. Under electron-beam radiation, nanobubbles smaller than 50 nm were generated by the electron-beam radiolysis process.

3. Results and discussion

3.1. Stability of nanobubbles: Effects of surfactants

Nanobubbles inside the nanochamber can be clearly identified in the *in situ* TEM images (Appendix A Movie S1). The circles with bright contrast and the surrounding area with dark contrast distinctly indicate the nanobubbles and liquid media, respectively, in Fig. 1(a). Nanobubbles were generated in different sizes, ranging from ~5 to ~30 nm, as shown in the first TEM image in Fig. 1(a). The nanobubbles can be categorized into two different types depending on their location in the nanochamber: Surface nanobubbles are located near the AAO wall and tend to adsorb onto the inner surface of the AAO pore, while bulk nanobubbles are located in the middle of the liquid media without surface adsorption. In general, the existence of nanobubbles follows the Young–Laplace equation; that is, the internal pressure (P_{in}) of the bubbles balances the sum of the pressure from the surrounding fluid (P_{out}) and the

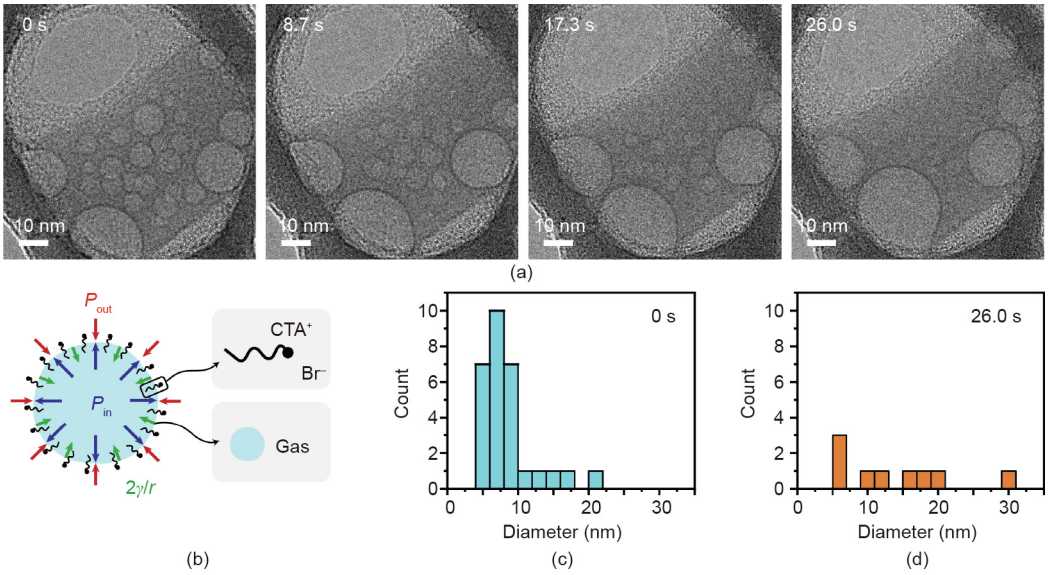

Fig. 1. (a) Time-series of TEM images showing nanobubbles in a nanochamber. (b) Illustration of a nanobubble in an aqueous CTAB solution. (c, d) Size distribution of the nanobubbles at (c) 0 s and (d) 26 s, as shown in part (a). CTA$^+$: hexadecyltrimethylammoniumcation; *r*: radius.

pressure created by surface tension (γ), as illustrated in Fig. 1(b). A time-series of TEM images of nanobubbles (Fig. 1(a)) exhibits the relative stabilities of the two different types of nanobubbles. The surface nanobubbles are generally larger and exhibit longer lifetimes than the bulk nanobubbles. In contrast, most of the bulk nanobubbles have a spherical shape, and small bulk nanobubbles continue to shrink over time, as shown in Fig. 1(a). The average diameter of the shrinking bulk nanobubbles was measured to be ~6 nm based on the time-series of the TEM images; it is also represented in the histogram of nanobubble diameters at 0 and 26 s (Figs. 1(c) and (d)). The critical radius of stable nanobubbles in pure water has been reported to be (6.3 ± 0.8) nm [35], which is approximately twice the value we observed in the aqueous CTAB solution. This result is probably due to the surface tension of the aqueous CTAB solution (33.59 $mN{\cdot}m^{-1}$) being significantly lower than that of pure water (72.8 $mN{\cdot}m^{-1}$) [29,32,38], implying that surfactants in the liquid media can form a layer between the gas-containing bubbles and the surrounding liquid, which stabilizes the gas–liquid interface of the nanobubbles [22,24]. Moreover, the presence of a sufficient amount of CTAB molecules (cationic surfactants) is likely to cause the nanobubbles to be positively charged due to the adsorption layer of CTAB, possibly stabilizing the nanobubbles by electrostatic pressure [22].

3.2. Gas transport via the interfacial region between nanobubbles

We investigated the interactions and gas transport behavior of surfactant-laden nanobubbles when they were in close proximity. In a typical bubble system ranging from the micrometer to nanometer scale, two interacting bubbles either merge or repel each other depending on their relative approach velocity, contact time, and surrounding fluid viscosity [39,40]. A merging event occurs via the destruction of the interfaces of the two bubbles, which results in the formation of a neck region through which gas migrates between the two bubbles. Such events, including gas transport followed by merging, have also been observed for nanobubbles in pure water [34,35]. However, surfactant-laden nanobubbles exhibit different behavior. Instead of forming a neck for gas transport, the two nanobubbles (NB1 and NB2) we observed in this study remain in proximity with a narrow inter-bubble distance while active gas transport proceeds, as shown in Fig. 2(a) and Appendix A Movie S2. The contours and projected area tracked for the two nanobubbles (Figs. 2(b) and (c)) indicate the rapid gas transport from NB1 to NB2 over a time interval of 6 s. The direction of gas transport is determined by the different Laplace pressures of the two nanobubbles, which are inversely proportional to the radius of their curvature. The gas moves from NB1, which has high internal pressure (smaller size), to NB2, which has low internal pressure (larger size). Due to this gas transport, NB1 shrinks and NB2 grows, which is similar to the Ostwald-ripening process. Meanwhile, the interfacial region between the two nanobubbles moves in the direction opposite to that of the gas transport (Fig. 2(b)), which probably results from the destruction of the original solid–liquid–gas three-phase contact line pinning while transferring kinetic energy by means of the transported gas molecules. We also measured the circularity of the two nanobubbles from their two-dimensional (2D) projected images. While the sizes of the two nanobubbles change during the gas transport, their circularity values remain constant at ~0.9, which means that their shapes remain spherical, as shown in Fig. 2(d). Maintaining circularity during gas transport has also been observed for nanobubbles in pure water systems, in which gas transport proceeds through an ultrathin water membrane [35]. The interesting feature of nanobubbles with surfactants present is that their surfaces are not fully in contact, with a spacing of (0.91 ± 0.045) nm during the gas transport, as shown in Fig. 2(e). The rigid structure of the surfactant molecules packed along the boundaries of the two nanobubbles and their positively charged surfaces presumably prohibit complete merging and maintain a narrow gap of less than 1 nm. It is difficult to preserve a bulk liquid structure in this narrow region, which results in local liquid media with a lowered density through which gas molecules can be transported. The gas transport eventually stops (after t_0 + 20 s, where t_0 is the time when the inter-bubble distance is less than 1.5 nm) as the surfaces of the nanobubbles move apart.

It was commonly observed that interacting surfactant-laden nanobubbles remain in close proximity with a narrow gap over an extended period of time. One more example that exhibited a similar interaction and gas transport between nanobubbles (NB1 and NB2) is shown in Fig. 3(a) and Appendix A Movie S3. Interestingly, after a long period of stable gas transport, NB1 and NB2 undergo rapid merging when their boundaries come into physical

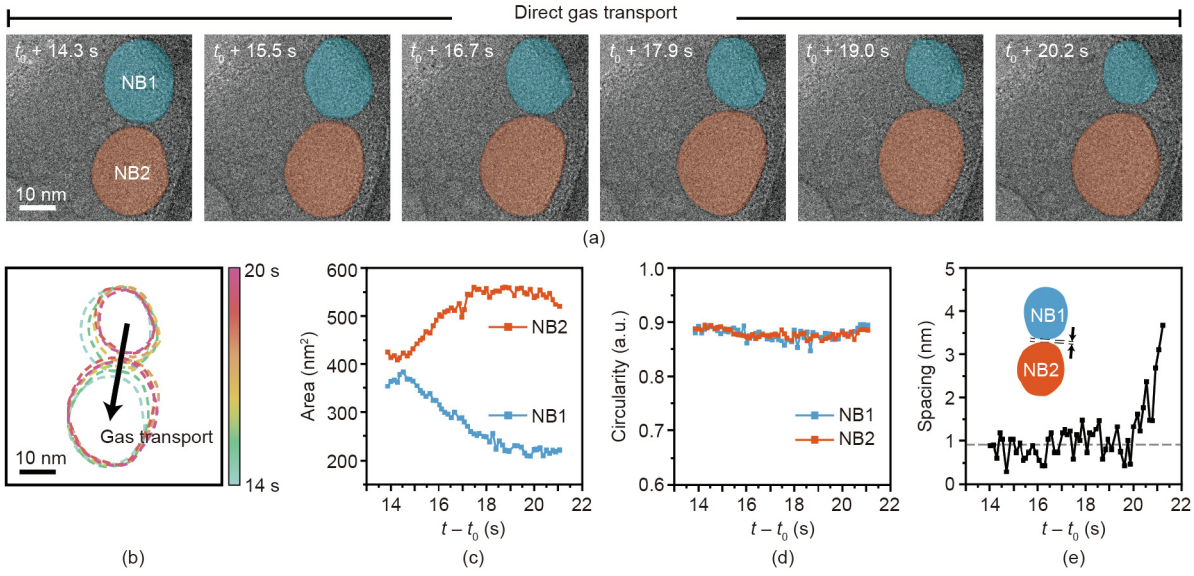

Fig. 2. (a) Time-series of TEM images indicating direct gas transport between two nanobubbles (NB1 and NB2). (b) Temporal trajectories for the contours of the two nanobubble boundaries. (c) Area and (d) circularity changes in time for the two tracked nanobubbles. (e) Tracked spacing between the boundaries of the two nanobubbles.

contact (Fig. 3(b)). The tracked contours and projected areas of the two nanobubbles (Figs. 3(c) and (d)) indicate that the gas is transmitted from the smaller NB1 to the larger NB2 for an initial 1.1 s (from NRF t_0 + 12.6 s to t_0 + 13.7 s). The small NB1 consistently shrinks, while the large NB2 grows, as the gas flows from the small to large nanobubble. During gas transport, the two nanobubbles maintain their spherical shape with a circularity of ~0.9, as shown in Fig. 3(e). When the spacing between the two nanobubbles is extremely close (below 0.5 nm), such that the effects of their interfacial fluctuations become significant, their gas–liquid interfaces are partially destroyed, and the nanobubbles begin to merge (Fig. 3(b)). After merging, the gas–liquid interface of the merged nanobubble quickly relaxes (Fig. 3(f)), and the nanobubble evolves into a spherical shape with a circularity of ~0.9 within 1.5 s (Fig. 3(e)).

3.3. Gas–liquid interface deformation by the formation of a flat boundary

The two nanobubbles shown in Fig. 4 also maintain their stable gap for a prolonged period of 6 s, which is consistent with the cases shown in Figs. 2 and 3 and Appendix A Movie S4. When the nanobubbles eventually merge, the merged nanobubble exhibits a non-spherical shape, having a concave surface. As the concave interface relaxes, an ellipsoidal-shaped nanobubble forms within a confined space, as shown in Fig. 4(a) and Appendix A Movie S5 [41]. The merged gas nanobubble maintains a stable ellipsoidal shape. This nanobubble has a flat gas–liquid interface, which is easily deformed by the surrounding liquid flux. The fluctuation of the deformed liquid–gas interface is shown in Fig. 4(c) as colored dashed lines. The time-series of TEM images in Fig. 4(b) shows the generation of a large number of ultrasmall nanobubbles from the collapsing flat interface of the ellipsoidal nanobubble. When the interface curvature becomes convex at a certain moment, while the interface of the nanobubble fluctuates in the presence of small bubbles in the bulk phase, the gas–liquid interface is transiently stabilized, as shown in Fig. 4(b). In the case of a nanobubble with a convex interface, because the radius of the interface curvature is on the nanometer scale, the internal pressure at the interface is high enough to balance the pressure from the surrounding liquid flow (Fig. 4(d)). Conversely, the internal pressure of the flat interface is comparable to the pressure of the surrounding liquid flow, which can facilitate the deformation of the gas–liquid interface. At this moment, small nanobubbles can easily be produced from the unstable gas–liquid interface under electron-beam radiation, as illustrated in Fig. 4(e). The sizes of the generated nanobubbles are mostly smaller than the critical size of stable nanobubbles; thus, the generated nanobubbles tend to rapidly lose their stability and dissolve.

3.4. The effects of electron-beam and chemical conditions on nanobubbles

During TEM observation, the radiolysis reaction of water induced by the electron beam can produce nanobubbles [31,42]. The stability of the generated nanobubbles may be reduced due to the high scattering of the electron beam at the gas–liquid interfaces. However, we believe that the use of graphene windows may help to avoid unwanted effects on our observations, since graphene has a better ability to reduce the electron-beam effect or damage and to scavenge reactive radical species than other conventional liquid cells with SiN_x windows [43,44]. Studies published recently by other groups have reported the poor stability of bulk

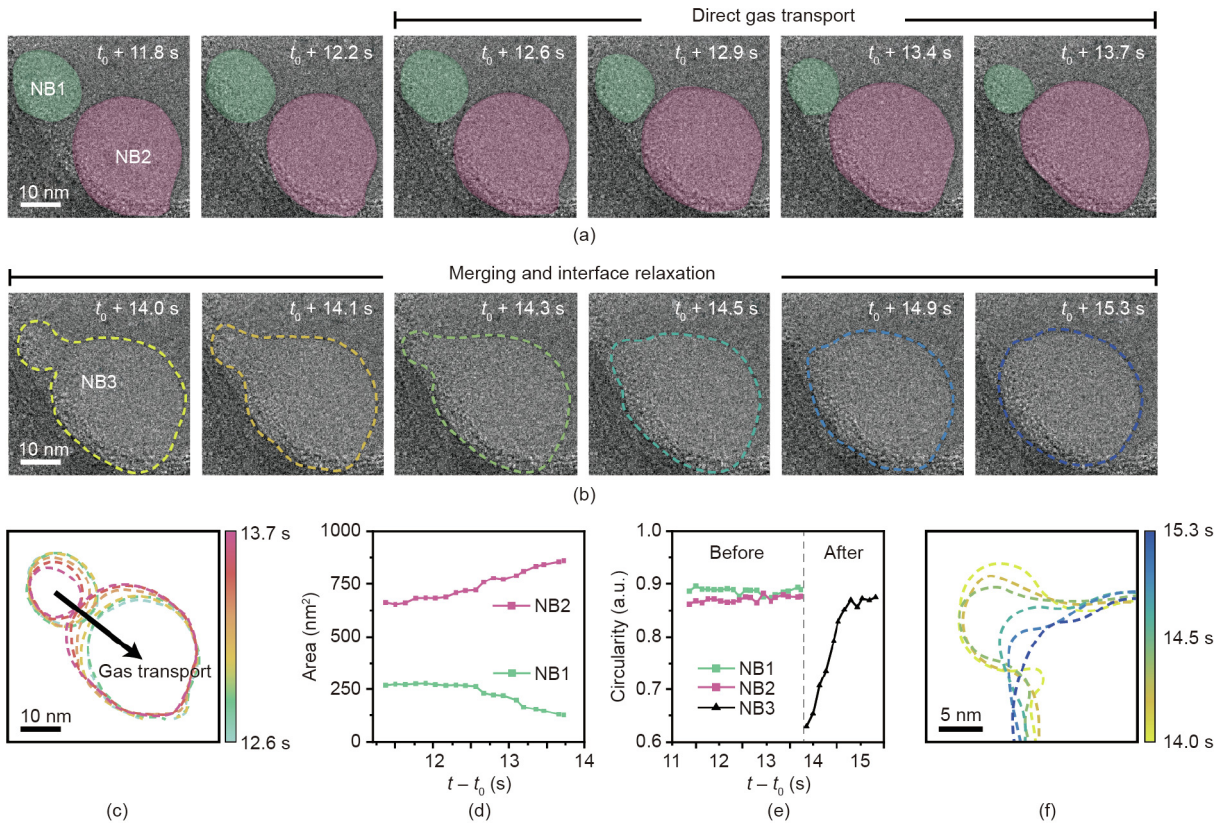

Fig. 3. Time-series of TEM images indicating (a) direct gas transport between two nanobubbles (NB1 and NB2) and (b) their merging process (NB3). (c) Contours of two nanobubble boundaries. (d) Change in area over time of two nanobubbles. (e) Tracked circularity of the nanobubbles before and after merging. (f) The local magnified contours of the merged nanobubble boundary.

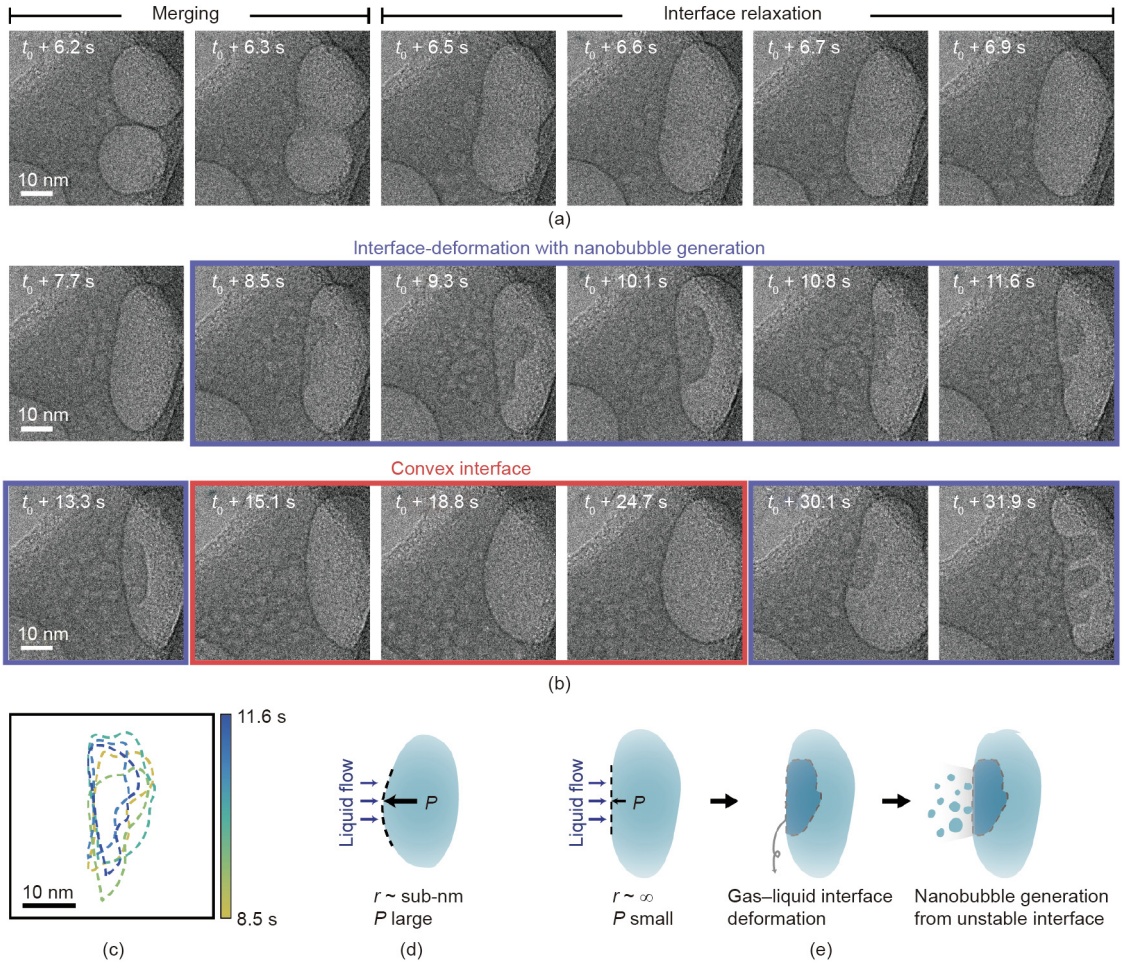

Fig. 4. (a) Time-series of TEM images showing the nanobubble merging and interface relaxation process. (b) Time-series of TEM images showing gas–liquid interface deformation and nanobubble generation from the unstable interface. (c) Magnified contours of the fluctuations of deformed gas–liquid interfaces. Illustration of the interfacial stability of a nanobubble depending on its curvature: (d) convex interface and (e) flat interface of an ellipsoidal nanobubble. *r*: radius of curvature.

nanobubbles in low-pH or salt solutions [45,46]. The pH of the observed system was around 2.16, and various salts existing in the system may influence the stability of the nanobubbles. Nevertheless, as shown in Fig. 1, the effect of surfactants on the stabilization of small nanobubbles seems to be predominant.

4. Conclusions

In summary, we performed TEM observations of surfactant-laden nanobubbles in a liquid phase by using multi-chamber graphene liquid cells. We investigated the inter-nanobubble dynamics, including direct gas transport and merging processes. Our results indicate that a certain distance between interacting surfactant-laden nanobubbles is maintained over a prolonged period of time while stable gas transport occurs, rather than interfacial rupture followed by a merging process. Real-time TEM observations of nanobubbles also revealed that the stability of the interface of the nanobubbles degrades as the curvature decreases. Our studies based on *in situ* liquid-phase TEM provide physical insight into the fluid dynamics of bubbles at the nanoscale. The experimental method introduced in this report can be extended to other systems, including foam/emulsion stabilization, acoustic cavitation, sonochemistry, water treatment, and programmable drug/gene delivery, thereby providing physical perspectives that facilitate their applications.

Acknowledgements

Yuna Bae, Sungsu Kang, Byung Hyo Kim, and Jungwon Park acknowledge the financial support from the National Research Foundation of Korea (NRF) grant funded by the Korean government (Ministry of Science and ICT; NRF-2017R1A5A1015365), Creative-Pioneering Researchers Program through Seoul National University (2020), the Interdisciplinary Research Initiatives Programs by College of Engineering and College of Medicine, Seoul National University, and the POSCO Science Fellowship of POSCO TJ Park Foundation. Kitaek Lim, Sungho Jeon, and Won Chul Lee acknowledge the support from the NRF funded by the Ministry of Education (2019R1F1A1059099 and 2020R1F1A1065856) and the support from the research fund of Hanyang University (HY-2018-N).

Compliance with ethics guidelines

Yuna Bae, Sungsu Kang, Byung Hyo Kim, Kitaek Lim, Sungho Jeon, Sangdeok Shim, Won Chul Lee, and Jungwon Park declare that they have no conflict of interest or financial conflicts to disclose.

Appendix A. Supplementary data

Supplementary data to this article can be found online at https://doi.org/10.1016/j.eng.2021.02.006.

References

[1] Zhu J, An H, Alheshibri M, Liu L, Terpstra PMJ, Liu G, et al. Cleaning with bulk nanobubbles. Langmuir 2016;32(43):11203–11.
[2] Agarwal A, Ng WJ, Liu Y. Principle and applications of microbubble and nanobubble technology for water treatment. Chemosphere 2011;84 (9):1175–80.
[3] Temesgen T, Bui TT, Han M, Kim TI, Park H. Micro and nanobubble technologies as a new horizon for water-treatment techniques: a review. Adv Colloid Interface Sci 2017;246:40–51.
[4] Atkinson AJ, Apul OG, Schneider O, Garcia-Segura S, Westerhoff P. Nanobubble technologies offer opportunities to improve water treatment. Acc Chem Res 2019;52(5):1196–205.
[5] Misra SK, Ghoshal G, Gartia MR, Wu Z, De AK, Ye M, et al. Trimodal therapy: combining hyperthermia with repurposed bexarotene and ultrasound for treating liver cancer. ACS Nano 2015;9(11):10695–718.
[6] Xing Z, Wang J, Ke H, Zhao B, Yue X, Dai Z, et al. The fabrication of novel nanobubble ultrasound contrast agent for potential tumor imaging. Nanotechnology 2010;21(14):145607.
[7] Zhang X, Chan DY, Wang D, Maeda N. Stability of interfacial nanobubbles. Langmuir 2013;29(4):1017–23.
[8] Alheshibri M, Qian J, Jehannin M, Craig VS. A history of nanobubbles. Langmuir 2016;32(43):11086–100.
[9] Kim E, Choe JK, Kim BH, Kim J, Park J, Choi Y. Unraveling the mystery of ultrafine bubbles: establishment of thermodynamic equilibrium for sub-micron bubbles and its implications. J Colloid Interface Sci 2020;570:173–81.
[10] Epstein PS, Plesset MS. On the stability of gas bubbles in liquid–gas solutions. J Chem Phys 1950;18(11):1505–9.
[11] Craig VSJ. Very small bubbles at surfaces—the nanobubble puzzle. Soft Matter 2011;7(1):40–8.
[12] Li D, Jing D, Pan Y, Wang W, Zhao X. Coalescence and stability analysis of surface nanobubbles on the polystyrene/water interface. Langmuir 2014;30 (21):6079–88.
[13] Hampton MA, Nguyen AV. Nanobubbles and the nanobubble bridging capillary force. Adv Colloid Interface Sci 2010;154(1–2):30–55.
[14] Li M, Tonggu L, Zhan X, Mega TL, Wang L. Cryo-EM visualization of nanobubbles in aqueous solutions. Langmuir 2016;32(43):11111–5.
[15] Hernandez C, Gulati S, Fioravanti G, Stewart PL, Exner AA. Cryo-EM visualization of lipid and polymer-stabilized perfluorocarbon gas nanobubbles—a step towards nanobubble mediated drug delivery. Sci Rep 2017;7(1):13517.
[16] Liu Y, Zhang X. Nanobubble stability induced by contact line pinning. J Chem Phys 2013;138(1):014706.
[17] Tan BH, An H, Ohl CD. Resolving the pinning force of nanobubbles with optical microscopy. Phys Rev Lett 2017;118(5):054501.
[18] Lohse D, Zhang X. Pinning and gas oversaturation imply stable single surface nanobubbles. Phys Rev E Stat Nonlin Soft Matter Phys 2015;91(3):031003.
[19] Kim JW, Lee D, Shum HC, Weitz DA. Colloid surfactants for emulsion stabilization. Adv Mater 2008;20(17):3239–43.
[20] Zhao CX, Chen D, Hui Y, Weitz DA, Middelberg APJ. Controlled generation of ultrathin-shell double emulsions and studies on their stability. ChemPhysChem 2017;18(10):1393–9.
[21] Haney B, Chen D, Cai LH, Weitz D, Ramakrishnan S. Millimeter-size Pickering emulsions stabilized with Janus microparticles. Langmuir 2019;35(13):4693–701.
[22] Nirmalkar N, Pacek AW, Barigou M. Interpreting the interfacial and colloidal stability of bulk nanobubbles. Soft Matter 2018;14(47):9643–56.
[23] Xiao Q, Liu Y, Guo Z, Liu Z, Zhang X. How nanobubbles lose stability: effects of surfactants. Appl Phys Lett 2017;111(13):131601.
[24] Nirmalkar N, Pacek AW, Barigou M. On the existence and stability of bulk nanobubbles. Langmuir 2018;34(37):10964–73.
[25] Ross FM. Liquid cell electron microscopy. Cambridge: Cambridge University Press; 2016.
[26] Kim BH, Yang J, Lee D, Choi BK, Hyeon T, Park J. Liquid-phase transmission electron microscopy for studying colloidal inorganic nanoparticles. Adv Mater 2018;30(4):1703316.
[27] De Yoreo JJ, Sommerdijk NAJM. Investigating materials formation with liquid-phase and cryogenic TEM. Nat Rev Mater 2016;1(8):1–18.
[28] Smith JW, Chen Q. Liquid-phase electron microscopy imaging of cellular and biomolecular systems. J Mater Chem B Mater Biol Med 2020;8(37):8490–506.
[29] Yang J, Alam SB, Yu L, Chan E, Zheng H. Dynamic behavior of nanoscale liquids in graphene liquid cells revealed by *in situ* transmission electron microscopy. Micron 2019;116:22–9.
[30] Tomo Y, Takahashi K, Nishiyama T, Ikuta T, Takata Y. Nanobubble nucleation studied using Fresnel fringes in liquid cell electron microscopy. Int J Heat Mass Transfer 2017;108:1460–5.
[31] Kim Q, Shin D, Park J, Weitz DA, Jhe W. Initial growth dynamics of 10 nm nanobubbles in the graphene liquid cell. Appl Nanosci 2018;11(1):1–7.
[32] Huang TW, Liu SY, Chuang YJ, Hsieh HY, Tsai CY, Wu WJ, et al. Dynamics of hydrogen nanobubbles in KLH protein solution studied with *in situ* wet-TEM. Soft Matter 2013;9(37):8856–61.
[33] White ER, Mecklenburg M, Singer SB, Aloni S, Regan BC. Imaging nanobubbles in water with scanning transmission electron microscopy. Appl Phys Express 2011;4(5):055201.
[34] Park JB, Shin D, Kang S, Cho SP, Hong BH. Distortion in two-dimensional shapes of merging nanobubbles: evidence for anisotropic gas flow mechanism. Langmuir 2016;32(43):11303–8.
[35] Shin D, Park JB, Kim YJ, Kim SJ, Kang JH, Lee B, et al. Growth dynamics and gas transport mechanism of nanobubbles in graphene liquid cells. Nat Commun 2015;6(1):6068.
[36] Lim K, Bae Y, Jeon S, Kim K, Kim BH, Kim J, et al. A large-scale array of ordered graphene-sandwiched chambers for quantitative liquid-phase transmission electron microscopy. Adv Mater 2020;32(39):e2002889.
[37] Regan W, Alem N, Alemán B, Geng B, Girit Ç, Maserati L, et al. A direct transfer of layer-area graphene. Appl Phys Lett 2010;96(11):113102.
[38] Shah SK, Chatterjee SK, Bhattarai A. Micellization of cationic surfactants in alcohol–water mixed solvent media. J Mol Liq 2016;222:906–14.
[39] Jiao J, He Y, Yasui K, Kentish SE, Ashokkumar M, Manasseh R, et al. Influence of acoustic pressure and bubble sizes on the coalescence of two contacting bubbles in an acoustic field. Ultrason Sonochem 2015;22:70–7.
[40] Postema M, Marmottant P, Lancée CT, Hilgenfeldt S, Jong Nd. Ultrasound-induced microbubble coalescence. Ultrasound Med Biol 2004;30(10):1337–44.
[41] Bala Subramaniam A, Abkarian M, Mahadevan L, Stone HA. Colloid science: non-spherical bubbles. Nature 2005;438(7070):930.
[42] Grogan JM, Schneider NM, Ross FM, Bau HH. Bubble and pattern formation in liquid induced by an electron beam. Nano Lett 2014;14(1):359–64.
[43] Cho H, Jones MR, Nguyen SC, Hauwiller MR, Zettl A, Alivisatos AP. The use of graphene and its derivatives for liquid-phase transmission electron microscopy of radiation-sensitive specimens. Nano Lett 2017;17(1):414–20.
[44] Zan R, Ramasse QM, Jalil R, Georgiou T, Bangert U, Novoselov KS. Control of radiation damage in MoS_2 by graphene encapsulation. ACS Nano 2013;7 (11):10167–74.
[45] Ke S, Xiao W, Quan N, Dong Y, Zhang L, Hu J. Formation and stability of bulk nanobubbles in different solutions. Langmuir 2019;35(15):5250–6.
[46] Hamamoto S, Takemura T, Suzuki K, Nishimura T. Effects of pH on nano-bubble stability and transport in saturated porous media. J Contam Hydrol 2018;208:61–7.